（3）CAPE的分布特征对上升气流的影响

上节课回顾

CAPE是浮力和积分厚度的函数，因而浮力的垂直分布对Updraft和风暴的强度有重要影响

1）CAPE形状 细长型vs. 矮胖型

1a. CAPE 相同时干空气的卷入在细长型CAPE情况下对对流层中层的上升流比在矮胖型CAPE的情况有更加明显的减弱作用。 干空气的卷入时间长，对浮力的减弱较明显。

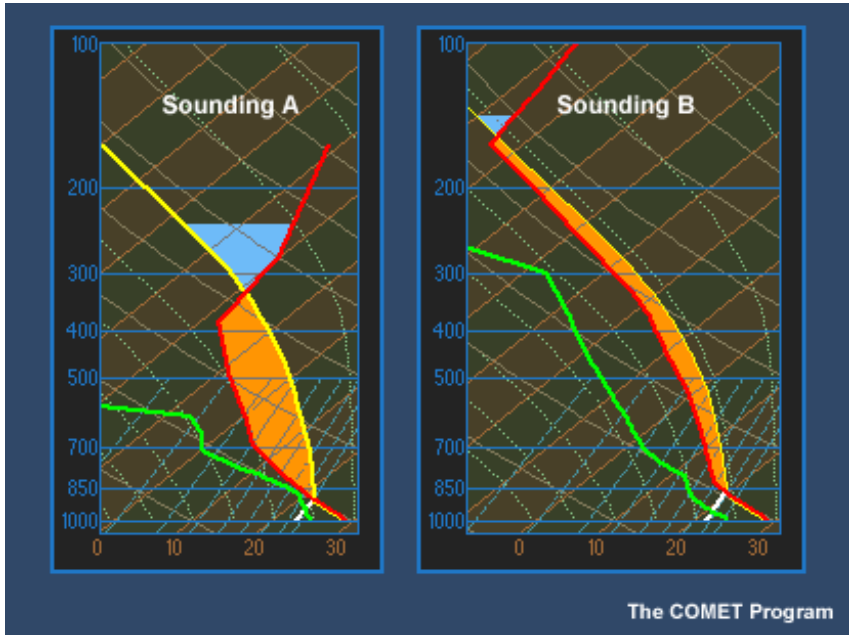

强天气往往对应中低层的强上升流。

（4）CAPE与气块的来源选择密切相关

上节课回顾

1） SBCAPE （Surface based CAPE）

随着地面温度升高， 对流一般会在午后起来，因而一般用预报的最高温度做温度订正

变率很大

高架对流时易低估CAPE

浅湿层时易高估CAPE

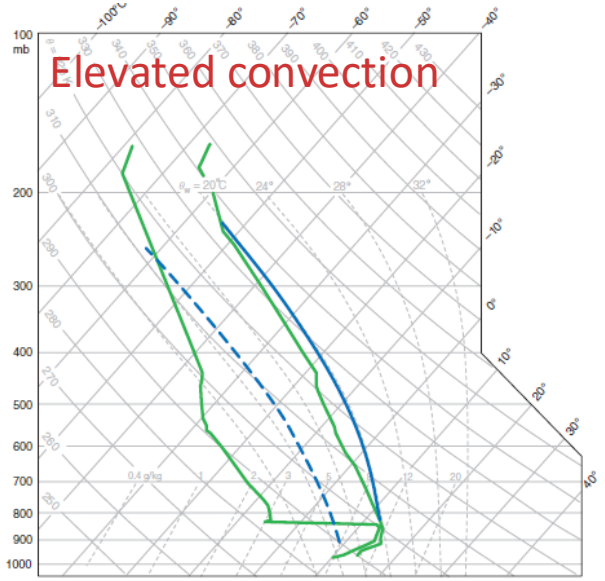

2） MLCAPE （Mixed layer CAPE）

气块始于平均层的中间位置

时空比较少变

有夜间浅层逆温时一般比SBCAPE大

混合较好时与SBCAPE接近

浅层逆温或浅湿层时较好用 。

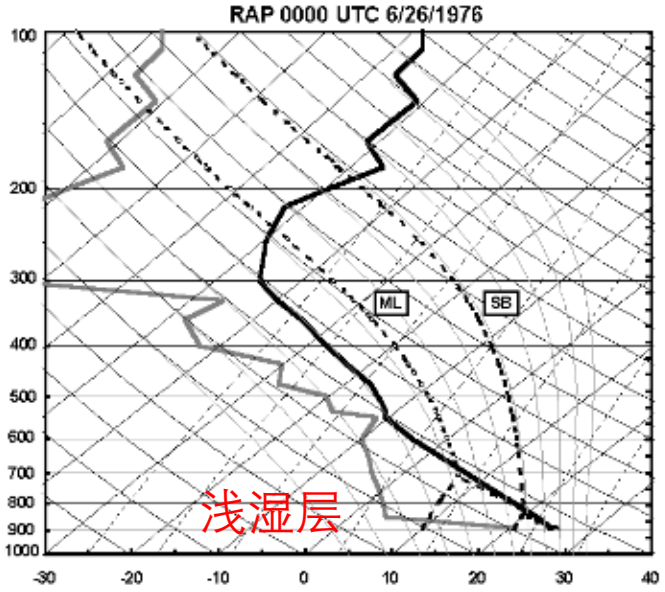

（4）CAPE与气块的来源选择密切相关

上节课回顾

FNL：地面–180 hPa的平均T和T_{d}

怀俄明学探空网站：地面–500 m 的平均T和T_{d}
（中国境内的站点于2019年1月20日被抹去）

3） MUCAPE （Most unstable CAPE）

在地面以上300 hPa层内找一个能得到最大CAPE的层次开始抬升

对高架对流较好用， SB、ML CAPE都会低估。

ERA5： 地面到300 hPa高度层之间的最大CAPE

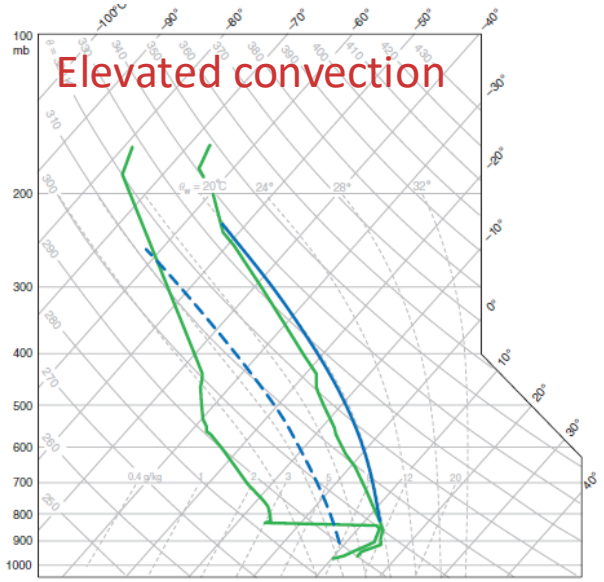

（5）水汽对CAPE的影响（虚温订正）

上节课回顾

$$\mathrm{CAPE_v} = \int_{z_{\mathrm{LFC}}}^{z_{\mathrm{EL}}} g \frac{(T_\mathrm{v})_\mathrm{p} - (T_\mathrm{v})_\mathrm{e}}{(T_\mathrm{v})_\mathrm{e}} dz$$

$$\frac{B}{g} = -\frac{\rho_\mathrm{g}'}{\overline{\rho_\mathrm{g}}} \approx \frac{T_\mathrm{v}'}{\overline{T_\mathrm{v}}} - \frac{p'}{\bar{p}} - q_\mathrm{h}$$

$$p = \rho \mathrm{R_d} T_\mathrm{v}$$

对湿空气，计算某一气压下的密度时，如果不调整$\mathrm{R_d}$，就需要用T_v

$$T_\mathrm{v} = T\ (1 + 0.608q)$$

订正步骤：

1）基于原始的T和T_d，画出气块绝热曲线

2）对环境温度和气块温度曲线做订正，湿度不做订正

3）基于订正后的曲线得到$\mathrm{CAPE_v}$、$\mathrm{CIN_v}$、$\mathrm{LFC_v}$、$\mathrm{EI_v}$，但是不改变LCL

（On using the virtual temperature correction by Chuck Doswell; Doswell and Rasmussen, WAF, 1994）

2.5 稳定度指数

上节课回顾

气块相对环境的温差，反映环境的稳定度，对流风暴发生的潜势

常用的几个指数： LI 抬升指数，TT指数， K指数

（1） LI（Lifting Index）

$$\mathrm{LI} = (T_e - T_p)_{500\ \mathrm{mb}}$$

单位：°C

负值表示不稳定

反映CAPE的大小

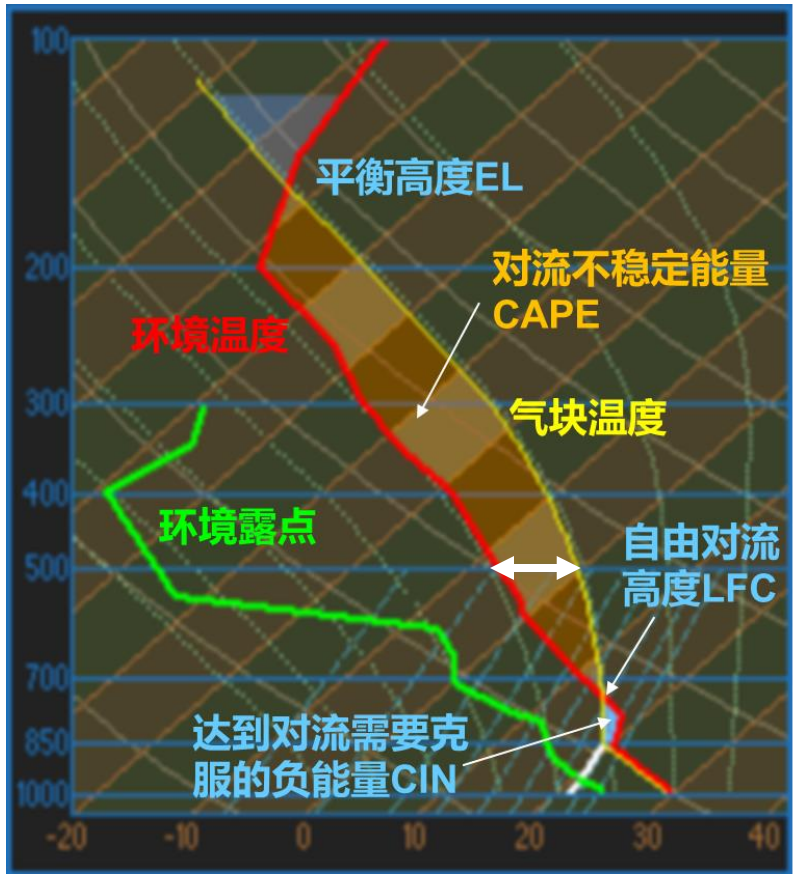

(2) Total – Totals Index (TT)

上节课回顾

$$\mathrm{TT} = T_{850} + T_{\mathrm{d}\,850} - 2T_{500}$$ 单位：℃ 均为环境温度

$$= \underbrace{T_{850} - T_{500}} + \underbrace{T_{\mathrm{d}\,850} - T_{500}}$$

Vertical totals (VT)

与环境减温率有关

Cross totals (CT)

包含了低层水汽的作用

Note： 湿层在850hPa以下时不太好用， 不能反映水汽的作用

（3）K指数

上节课回顾

$$K = (T_{850} - T_{500}) + T_{d\,850} - (T_{700} - T_{d\,700})$$ 单位：℃

1） K指数基于850–500 hPa之间的环境Υ、对流层低层的水汽含量、湿层的垂直范围

2）湿层在700 hPa以下不太适用

对于较小的K（<30），$T_{700} - T_{d\,700}$可能很大，但700 hPa以下可能很湿，整层抬升可能发生对流，称为对流不稳定。

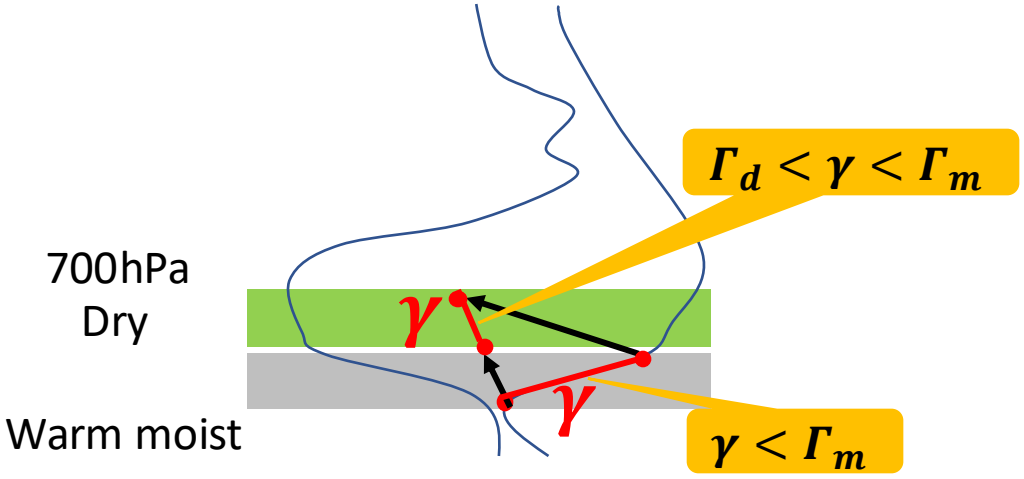

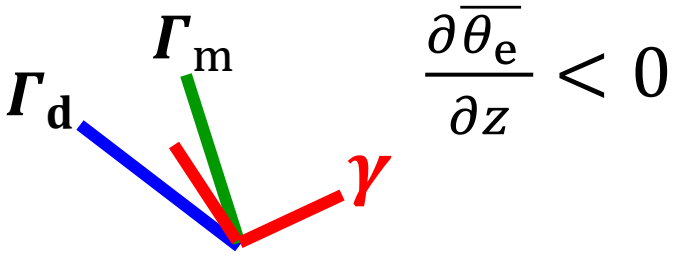

$$\frac{\partial \overline{\theta_e}}{\partial z} < 0$$

整层抬升，低层湿空气减温慢，高层干空气减温快，γ增大，导致不稳定

（2） CIN （Convective Inhibition）

上节课回顾

对流抑制：把空气块从地面抬升到LFC需要做的功。

用于描述Capping inversion的强度

$$B \equiv g\frac{T_\mathrm{p}-T_\mathrm{e}}{T_\mathrm{e}} \qquad T_\mathrm{p} < T_\mathrm{e},\ B < 0, \text{气块下沉}$$

1）**Skew-T计算**

在Skew-T上，相当于环境温度廓线和从地面(sfc)到LCL的干绝热线与从LCL到LFC的湿绝热线之间的负面积。

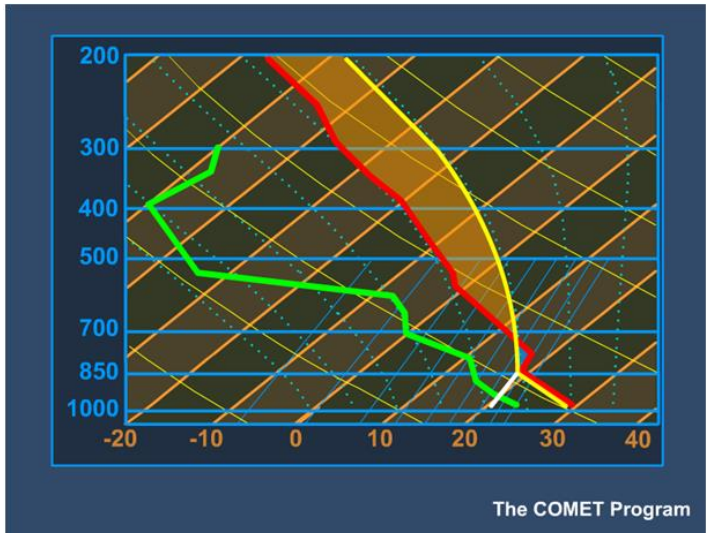

数学上是负值，实际应用一般只提它的绝对值。

$$\mathrm{CIN} \equiv \int_{z=\mathrm{sfc}}^{z=\mathrm{LFC}} B\,dz = g\int_{z=\mathrm{sfc}}^{z=\mathrm{LFC}} \frac{T_\mathrm{p}-T_\mathrm{e}}{T_\mathrm{e}}\,dz$$

So far, we discussed static instability (vertical acceleration) through parcel theory

$$\frac{dw}{dt} = B,$$

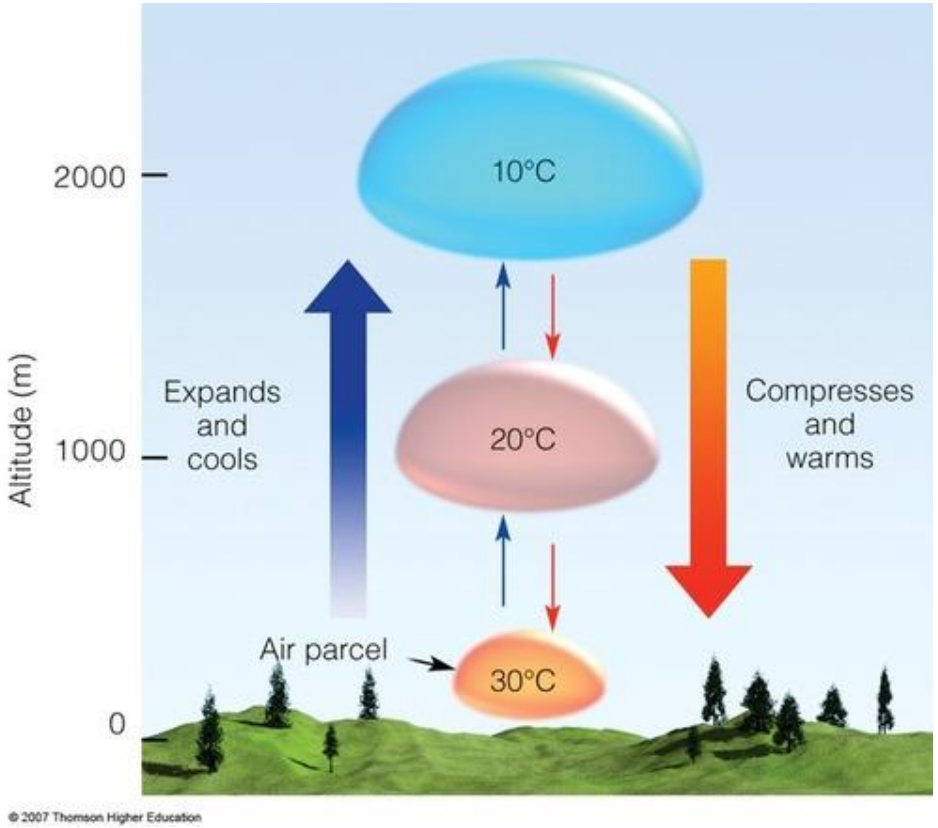

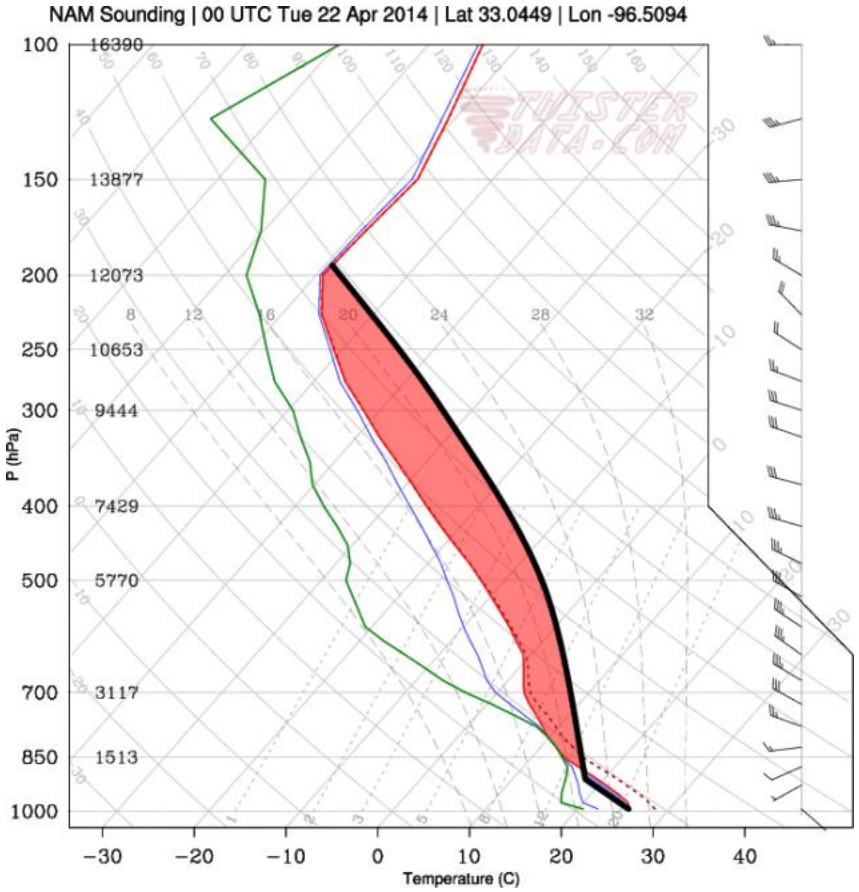

Neglecting the following
1) pressure perturbation
2) entrainment
3) hydrometeors
4) subsidence

1. pressure perturbation

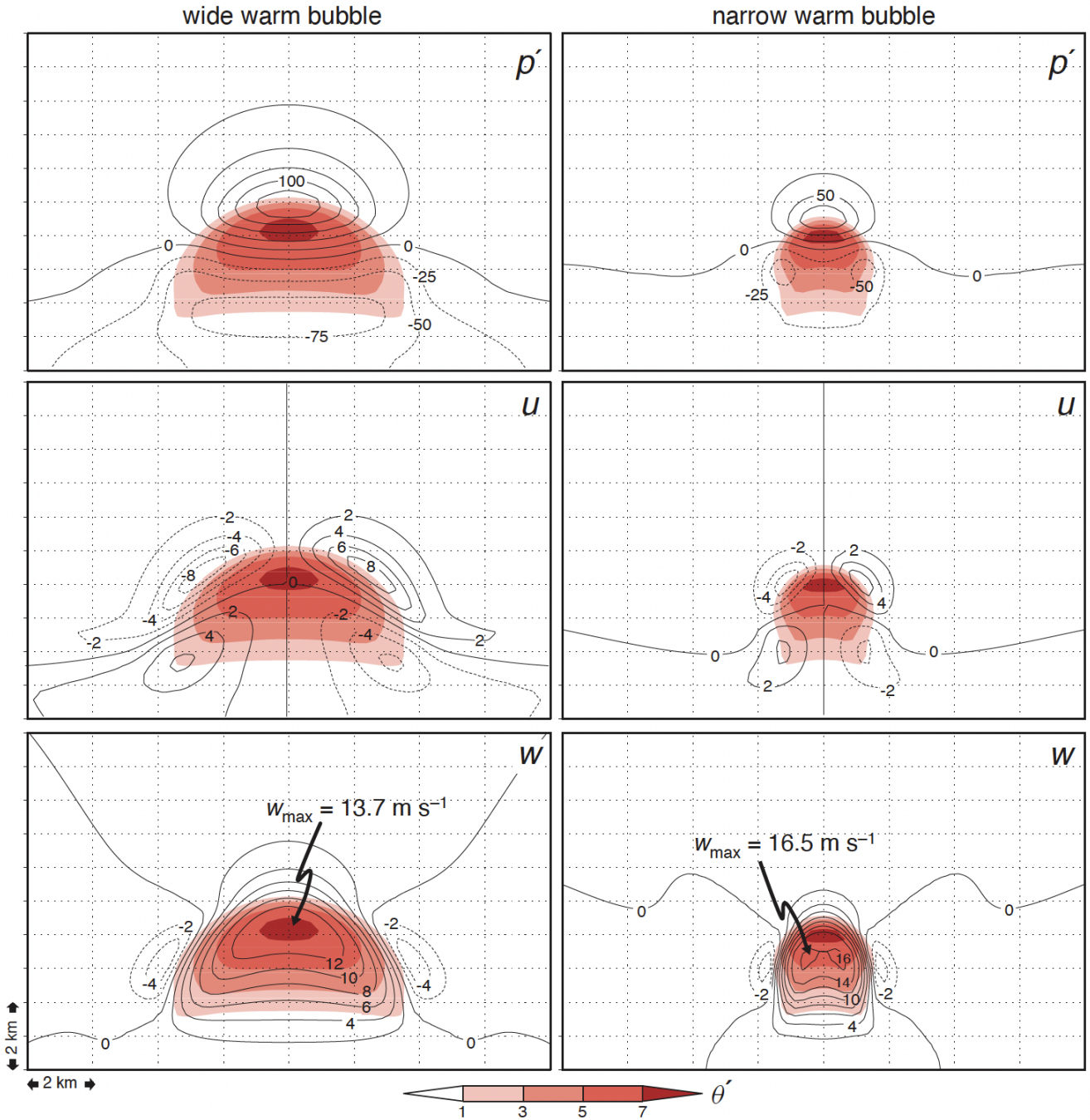

Figure 3.1 A comparison of the perturbation pressure (p') fields and zonal (u) and vertical (w) velocity components for the case of a wide warm bubble (left panels) and a narrow warm bubble (right panels) released in a conditionally unstable atmosphere in a three-dimensional numerical simulation. The contour intervals for p' and the wind components are 25 Pa and 2 m s^{-1}, respectively (dashed contours are used for negative values). Potential temperature perturbations (θ') are shown in each panel (refer to the color scale). The horizontal and vertical grid spacing is 200 m (the domain shown above is much smaller than the actual model domain). Both warm bubbles had an initial potential temperature perturbation of 2 K and a vertical radius of 1.5 km, and were released 1.5 km above the ground. The wide (narrow) bubble had a horizontal radius of 10 km (3 km). In the simulation of the wide (narrow) bubble, the fields are shown 800 s (480 s) after its release. The fields are shown at times when the maximum buoyancies are comparable. Despite the comparable buoyancies, the narrow updraft is 20% stronger owing to the weaker adverse vertical pressure gradient.

2. entrainment

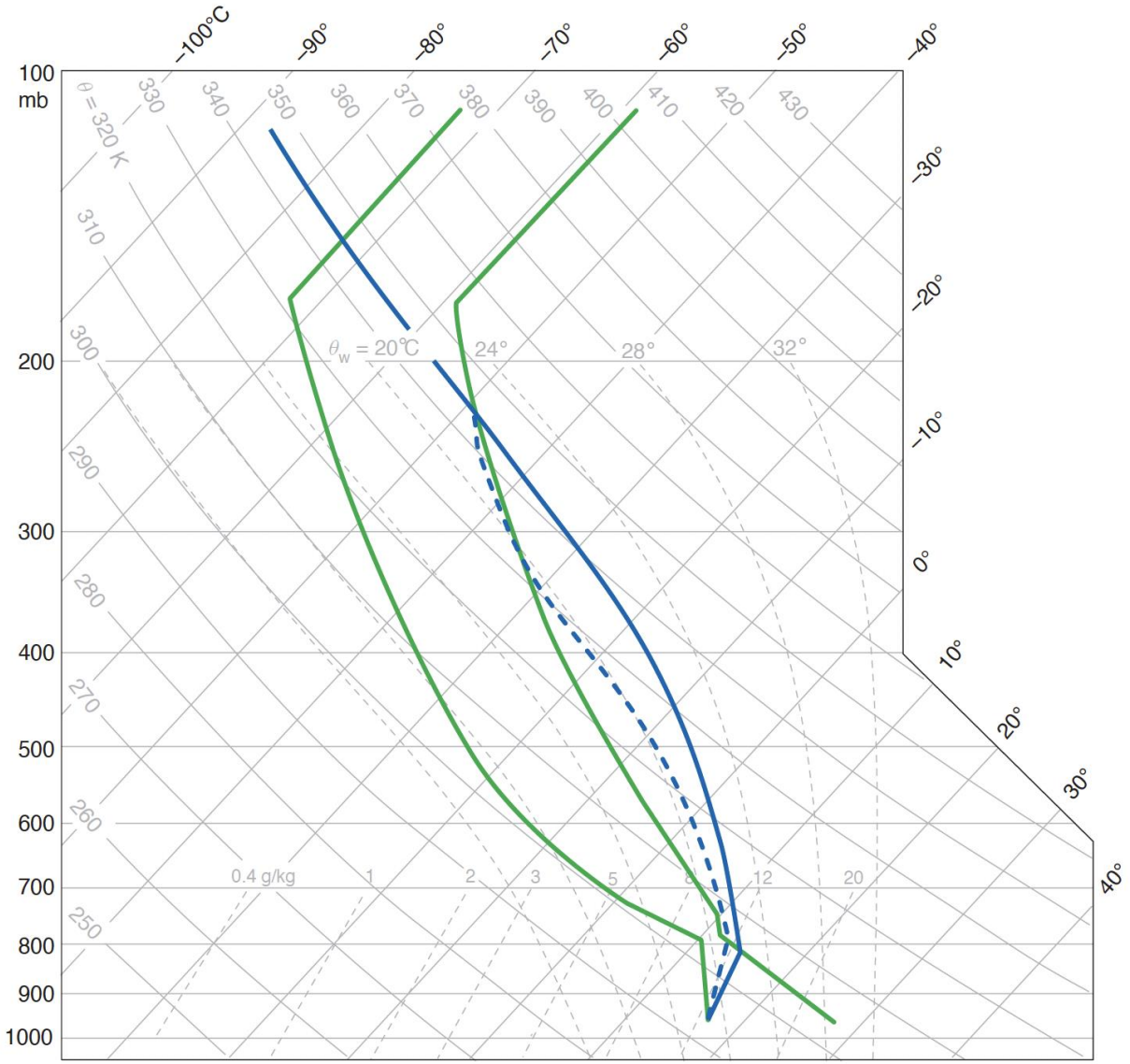

Figure 3.2 A possible parcel process curve (dashed) that might be followed by an updraft parcel on a skew T–log p diagram as a result of the entrainment of environmental air. A parcel process curve (solid) followed by an updraft parcel that ascends undiluted is also shown. Note the implied differences in cloud base (there has been some entrainment below the cloud base, in addition to entrainment over the cloud depth), cloud top, and the realized CAPE.

$$\frac{B}{g} \approx \frac{\theta'}{\overline{\theta}} + 0.61 q_v' - \frac{c_v}{c_p}\frac{p'}{\bar{p}} - q_h$$

升温1K对浮力的贡献相当于：增加5–6 g/kg 的水汽

减小3–4 hPa的气压

减小 3.3 g/kg的Water loading

4. subsidence

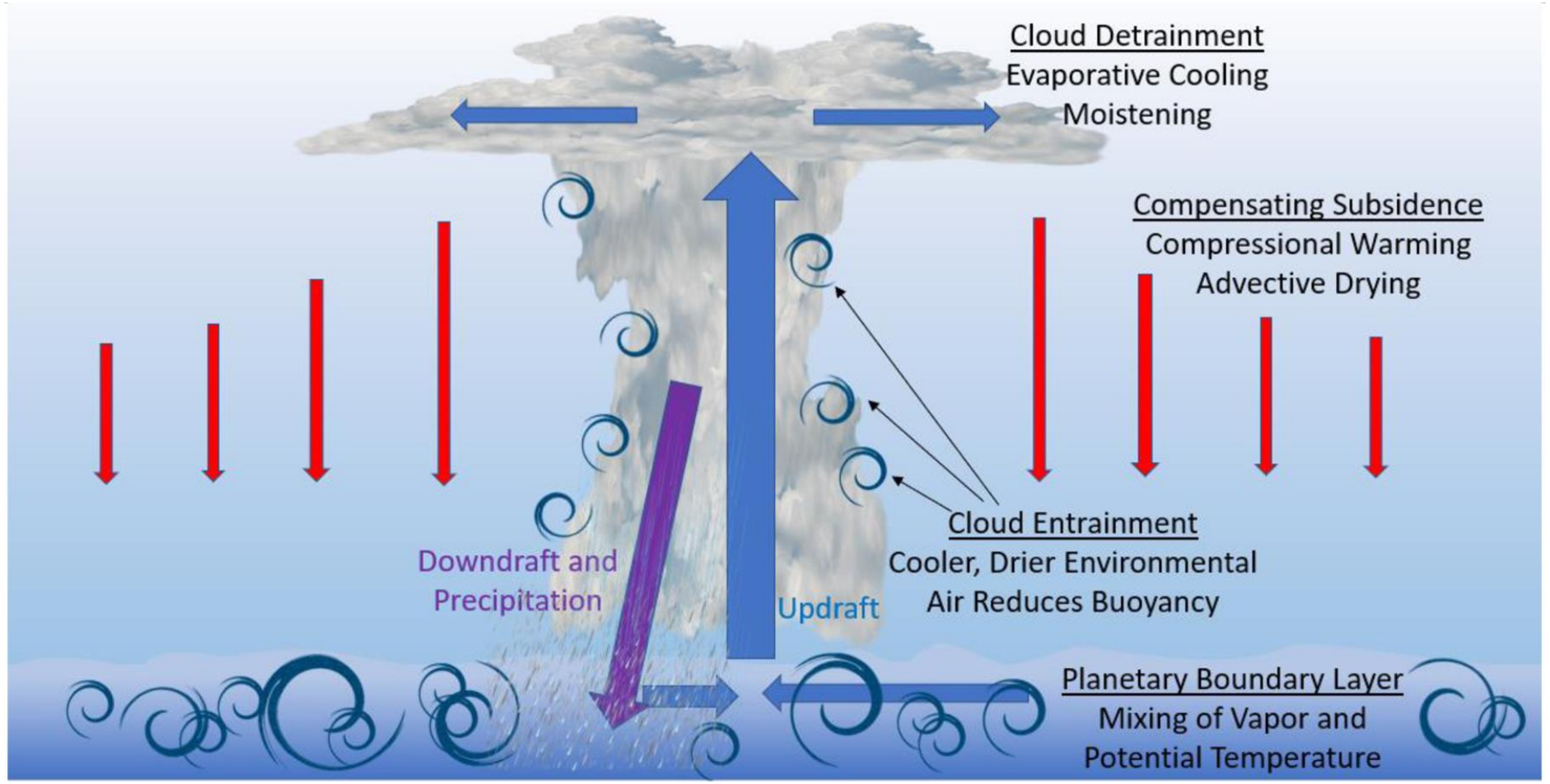

Centrifugal Instability (horizontal acceleration)

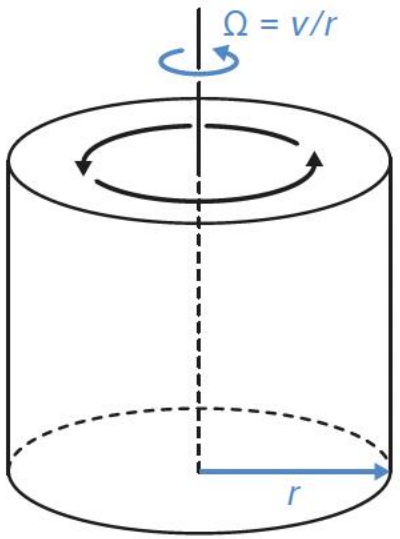

Figure 3.4 A cylindrical tank of spinning fluid, spinning at an angular velocity of $\Omega = v/r$.

The equations of horizontal motion in cylindrical coordinates are

$$\frac{\mathrm{d}u}{\mathrm{d}t} = -\alpha_0 \frac{\partial p}{\partial r} + \frac{v^2}{r} \tag{3.19}$$

$$\frac{\mathrm{d}(vr)}{\mathrm{d}t} = -\alpha_0 \frac{\partial p}{\partial \theta} \tag{3.20}$$

If we assume pressure field is symmetric,

$$\frac{\mathrm{d}u}{\mathrm{d}t} = -\alpha_0 \frac{\partial p}{\partial r} + \frac{M^2}{r^3} \tag{3.21}$$

$$\frac{\mathrm{d}M}{\mathrm{d}t} = 0. \tag{3.22}$$

the angular momentum $M = vr$,

Let us define a mean state and consider its perturbations

Let us define a mean state such that no radial acceleration exists and the horizontal pressure gradient force and centrifugal force balance each other:

$$0 = -\alpha_0 \frac{\partial \overline{p}}{\partial r} + \frac{\overline{M}^2}{r^3}. \tag{3.23}$$

Subtracting (3.24) from (3.22) gives

$$\frac{\mathrm{d}u}{\mathrm{d}t} = -\alpha_0 \frac{\partial p'}{\partial r} + \frac{1}{r^3}(M^2 - \overline{M}^2), \tag{3.24}$$

where $p = \overline{p} + p'$ and $M = \overline{M} + M'$. If we neglect the effects of the perturbation pressure gradient, as is done in parcel theory, we obtain

$$\frac{\mathrm{d}u}{\mathrm{d}t} = \frac{1}{r^3}(M^2 - \overline{M}^2). \tag{3.25}$$

The square of the mean angular momentum at the location of the displaced ring is (using a first-order Taylor series approximation)

$$\overline{M}^2 = M_0^2 + \frac{\mathrm{d}\overline{M}^2}{\mathrm{d}r}\Delta r, \tag{3.26}$$

where M_0 is the value of $\overline{M}$ at $r = r_0$. Also, because M^2 is conserved, its value for parcels within the displaced ring is

$$M^2 = M_0^2; \tag{3.27}$$

that is, a ring of fluid in equilibrium at r_0 retains its M^2 when displaced to $r_0 + \Delta r$. Therefore, for small Δr, and noting that $\mathrm{d}u/\mathrm{d}t = \mathrm{d}(\mathrm{d}r/\mathrm{d}t)/\mathrm{d}t = \mathrm{d}^2\Delta r/\mathrm{d}t^2$, (3.25) becomes

$$\frac{\mathrm{d}^2\Delta r}{\mathrm{d}t^2} = \frac{M^2 - \overline{M}^2}{(r_0 + \Delta r)^3} \tag{3.28}$$

$$\approx \frac{M_0^2 - \left(M_0^2 + \dfrac{\mathrm{d}\overline{M}^2}{\mathrm{d}r}\Delta r\right)}{r_0^3} \tag{3.29}$$

$$= -\frac{1}{r_0^3}\frac{\mathrm{d}\overline{M}^2}{\mathrm{d}r}\Delta r. \tag{3.30}$$

The general solution of (3.31) is

$$\Delta r(t) = C_1 \mathrm{e}^{i\left[\frac{1}{r_0^3}\frac{\mathrm{d}\overline{M}^2}{\mathrm{d}r}\right]^{1/2} t} + C_2 \mathrm{e}^{-i\left[\frac{1}{r_0^3}\frac{\mathrm{d}\overline{M}^2}{\mathrm{d}r}\right]^{1/2} t}, \tag{3.31}$$

Tornado

Hurricane

Inertial Instability (horizontal acceleration)

Let us consider the simple case of a zonal geostrophic wind that varies in the north-south (y) direction, that is, $u_g = u_g(y)$ and $v_g = 0$. Using a similar methodology as for the centrifugal stability analysis, we start with the horizontal equations of motion in Cartesian coordinates. In this case, they can be written as

$$\frac{du}{dt} = fv \tag{3.32}$$

$$\frac{dv}{dt} = f(u_g - u). \tag{3.33}$$

The variables u and v are the actual velocity components, which may include an ageostrophic component.

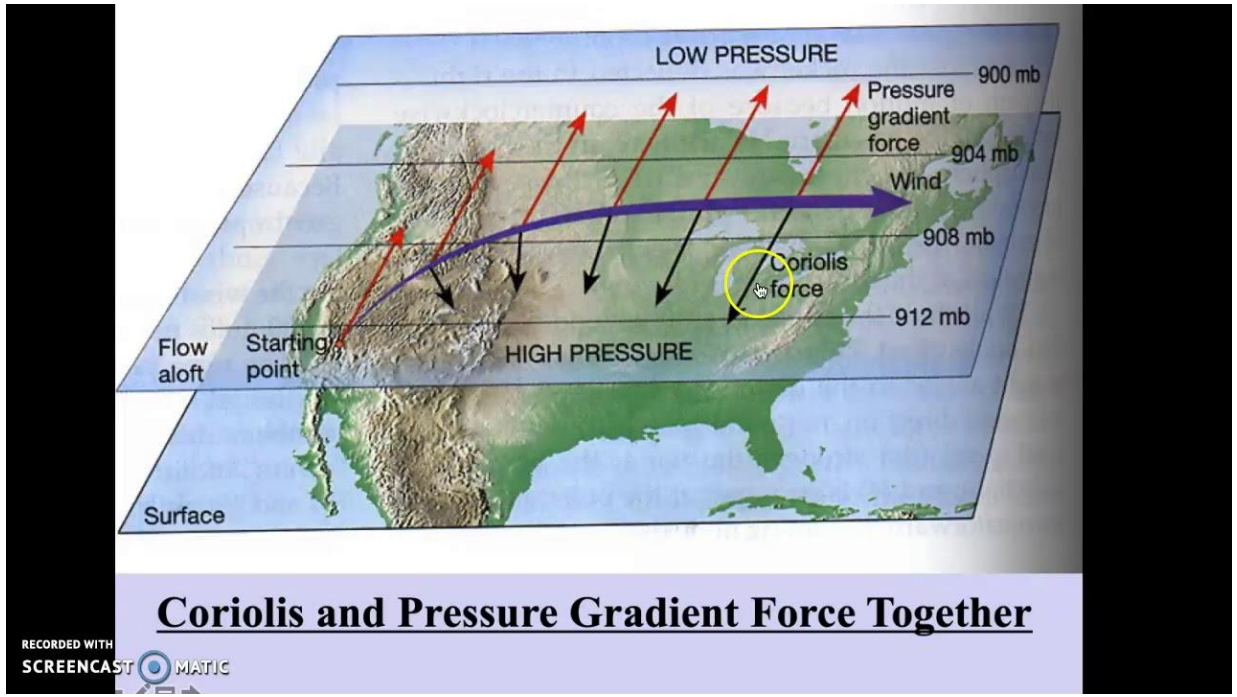

$$\frac{du}{dt} = fv \tag{3.32}$$

$$\frac{dv}{dt} = f(u_g - u). \tag{3.33}$$

The variables u and v are the actual velocity components, which may include an ageostrophic component.

The term $f - \partial u_g/\partial y$ is the absolute geostrophic vorticity (recall $v_g = 0$, so there is no $\partial v_g/\partial x$ term in the relative vorticity), and the general solution of (3.39) is

$$\Delta y(t) = C_1 e^{i\left[f\left(f-\frac{\partial u_g}{\partial y}\right)\right]^{1/2} t} + C_2 e^{-i\left[f\left(f-\frac{\partial u_g}{\partial y}\right)\right]^{1/2} t}, \tag{3.40}$$

Because $v \equiv dy/dt$, we can rev

$$\frac{du}{dt} = f\frac{dy}{dt} \tag{3.34}$$

$$\frac{d^2\Delta y}{dt^2} = f(u_g - u), \tag{3.35}$$

where Δy is the horizontal displacement distance from the initial position (i.e., $y = y_0 + \Delta y$ at some future time; thus, dy/dt can be written as $d\Delta y/dt$).

If the tube is displaced northward or southward, the new zonal velocity for a parcel within the tube will be, via integration of (3.34),

$$u = u_0 + f\Delta y. \tag{3.36}$$

Most readers are probably familiar with the above result in that it implies that a parcel moving northward (southward) is accelerated eastward (westward) owing to the mentum.
he location of the displaced tube
aylor series approximation)

$$+ \frac{\partial u_g}{\partial y}\Delta y. \tag{3.37}$$

initial pressure field and, correspondingly, the geostrophic wind, is not altered by the displacement of the tube. By subtracting (3.36) from the above expression, we obtain

$$u_g - u = \left(\frac{\partial u_g}{\partial y} - f\right)\Delta y, \tag{3.38}$$

and using (3.36), we obtain

$$\frac{d^2\Delta y}{dt^2} + f\left(f - \frac{\partial u_g}{\partial y}\right)\Delta y = 0. \tag{3.39}$$

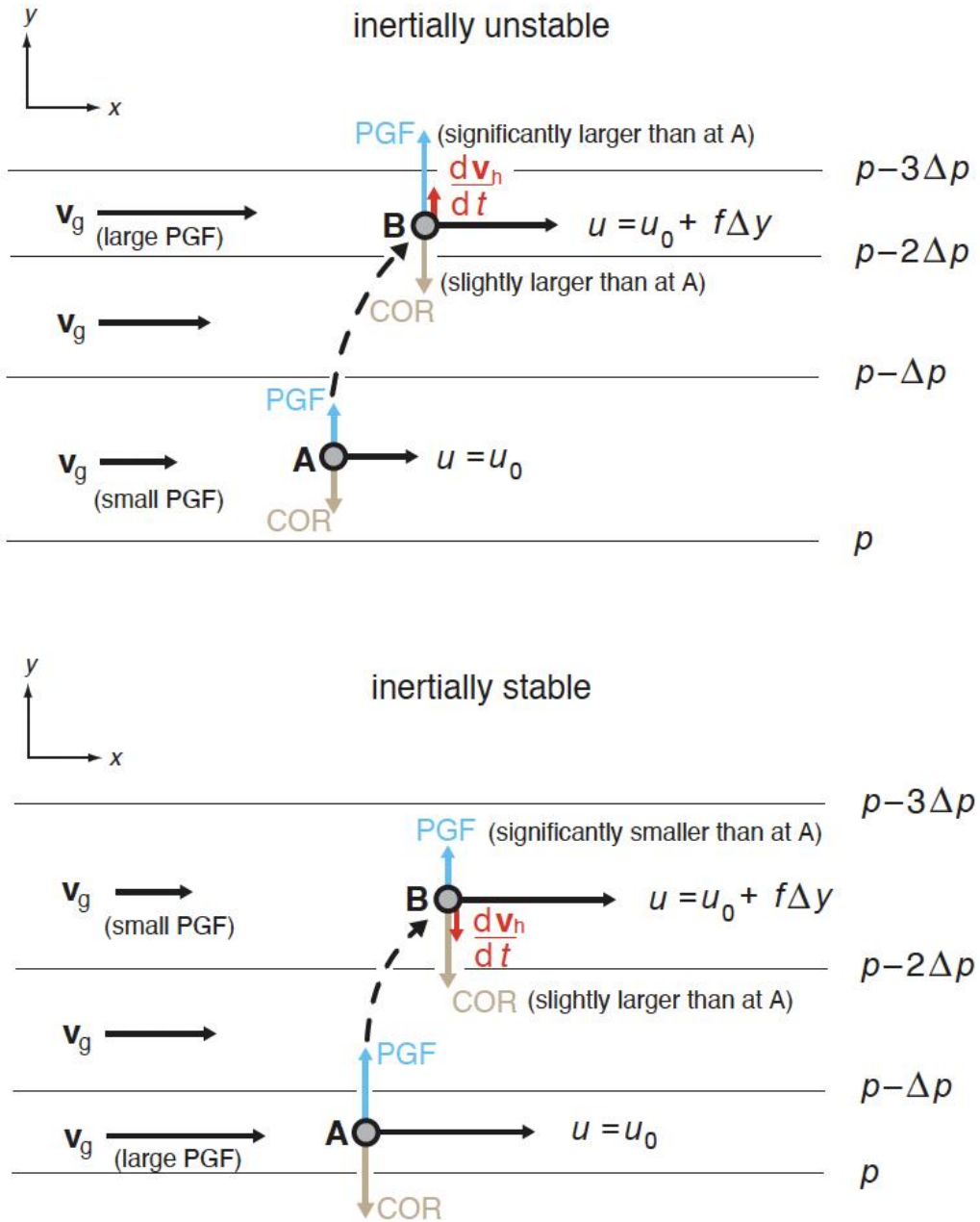

Figure 3.5 Top, the inertially unstable case, as discussed in the text. The parcel has been displaced northward, from point A to point B, as indicated by the dashed arrow. For clarity, only one parcel within the tube of displaced parcels is shown. Bottom, the inertially stable case.

balance, we define the *geostrophic absolute momentum* (or *geostrophic pseudoangular momentum*) as

$$M_g \equiv u_g - fy. \tag{3.42}$$

By inspection of (3.41) and noting that

$$-\frac{\partial M_g}{\partial y} = f - \frac{\partial u_g}{\partial y}, \tag{3.43}$$

inertial instability is present when $\partial M_g/\partial y > 0$. In this case,

Symmetric Instability (horizontal acceleration)

[11] The term *symmetric instability* appears to have originated from studies of centrifugal instability in a rotating tank with baroclinity carried out by H. Solberg (circa 1930). A *symmetric flow* is one in which the base state and perturbations only vary in two dimensions.

Air parcels can be both statically and inertially stable (i.e., in hydrostatic and geostrophic equilibrium, and therefore in thermal wind balance), but can be unstable to displacements along a path that is slanted with respect to the horizontal for certain distributions of geostrophic momentum and potential temperature. This type of instability is called *symmetric instability*.[11] Before embarking on the

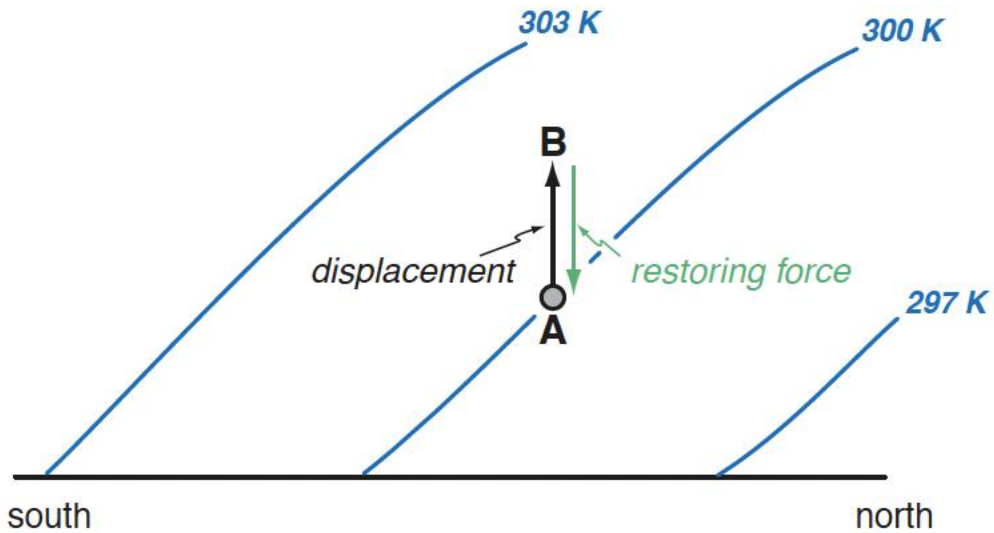

Figure 3.7 Schematic meridional cross-section of $\overline{\theta}$ surfaces in a statically stable atmosphere. A parcel that is displaced from position A toward position B experiences a restoring force that is directed toward its original equilibrium position.

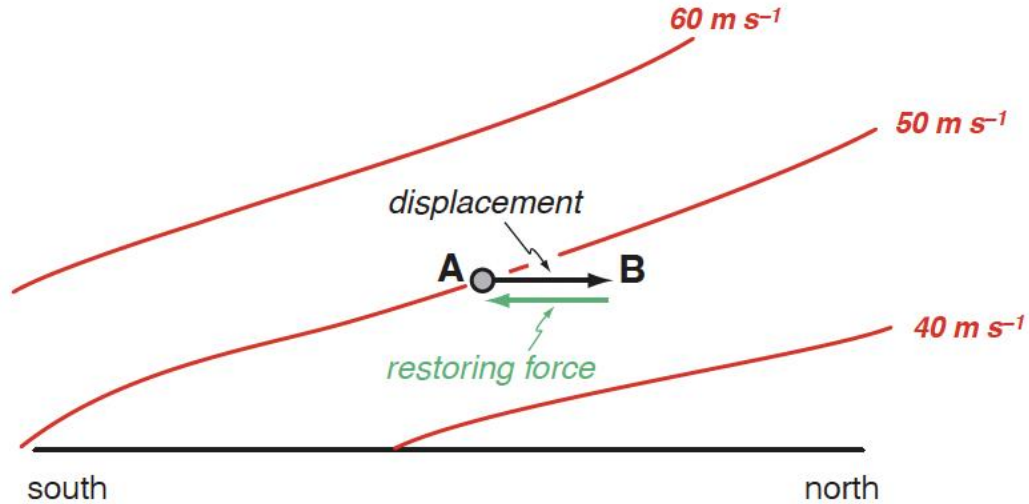

Figure 3.8 Schematic meridional cross-section of geostrophic absolute momentum surfaces in an inertially stable atmosphere. A tube of parcels that is displaced from position A toward position B experiences a restoring force that is directed toward its original equilibrium position.

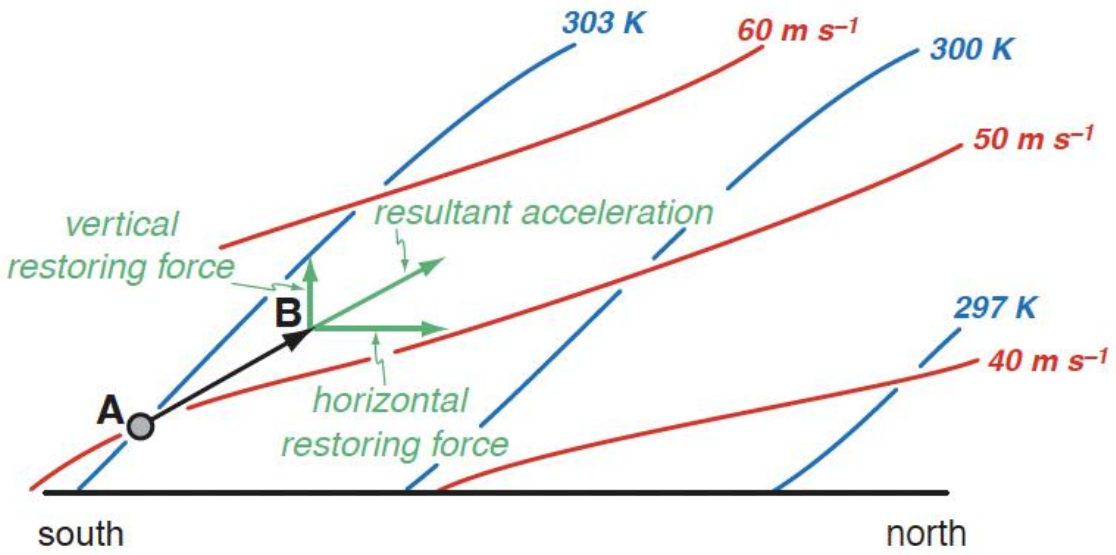

Figure 3.9 Schematic meridional cross-section of isentropic (blue) and geostrophic momentum surfaces (red) in a symmetrically unstable atmosphere. A tube of parcels that is displaced from position A toward position B experiences a resultant acceleration that is directed away from the original equilibrium position.

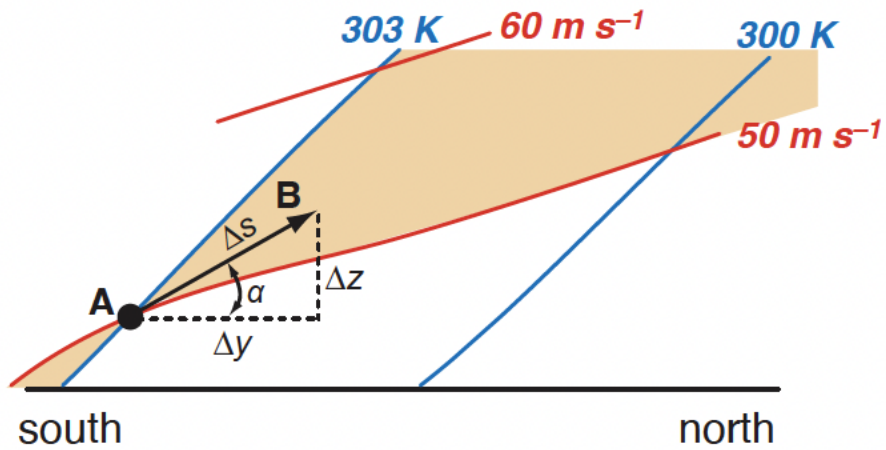

Figure 3.10 Zoomed-in view of Figure 3.9, showing the relationship between α, Δs, Δy, and Δz. Displacements of the parcel at position A to locations within the shaded region (e.g., toward position B) result in acceleration away from position A.

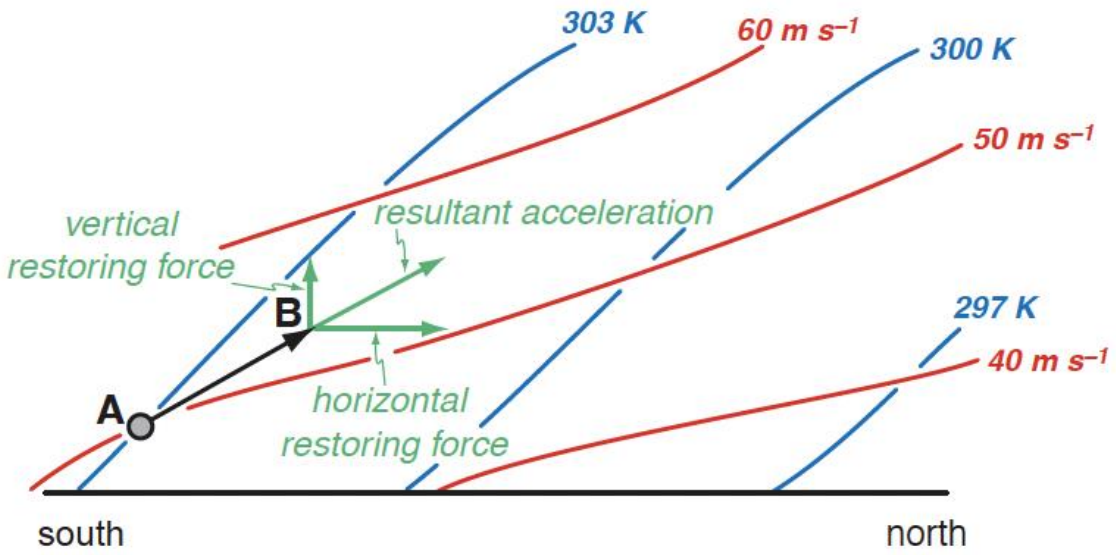

Figure 3.9 Schematic meridional cross-section of isentropic (blue) and geostrophic momentum surfaces (red) in a symmetrically unstable atmosphere. A tube of parcels that is displaced from position A toward position B experiences a resultant acceleration that is directed away from the original equilibrium position.

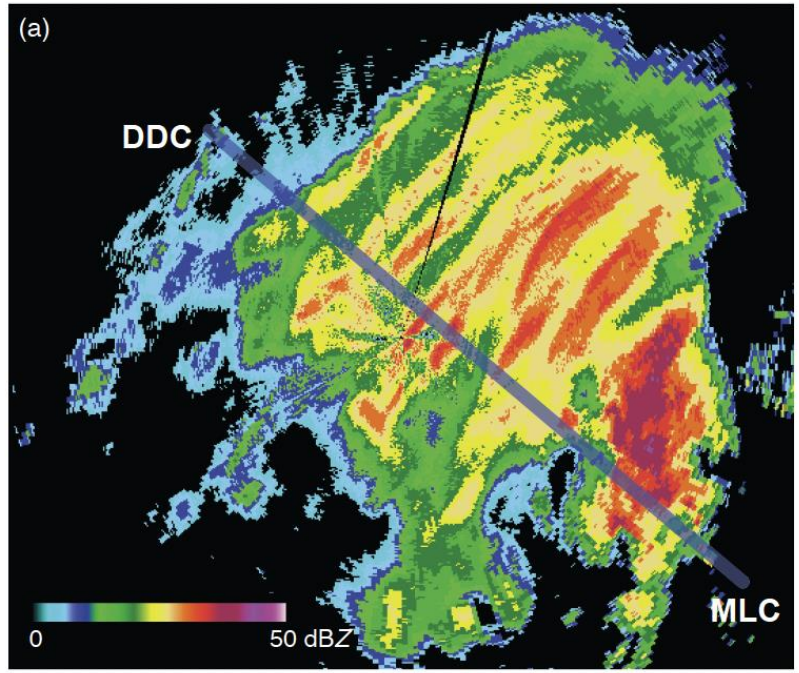

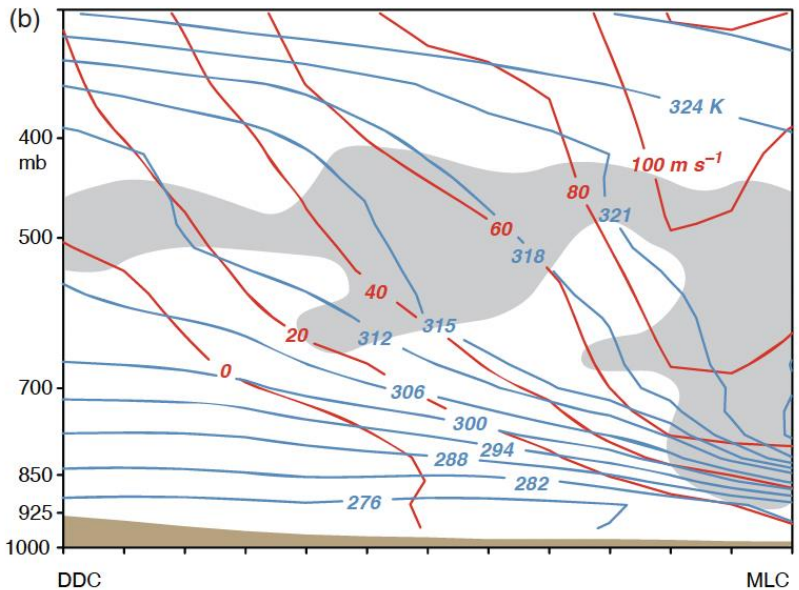

Shear Instability (stability of parallel flows)

Figure 3.12 Billow clouds, which resemble breaking waves, are a visual manifestation of vertical shear instability (also known as Kelvin–Helmholtz instability) when sufficient moisture is present. Photograph by Brooks Martner.

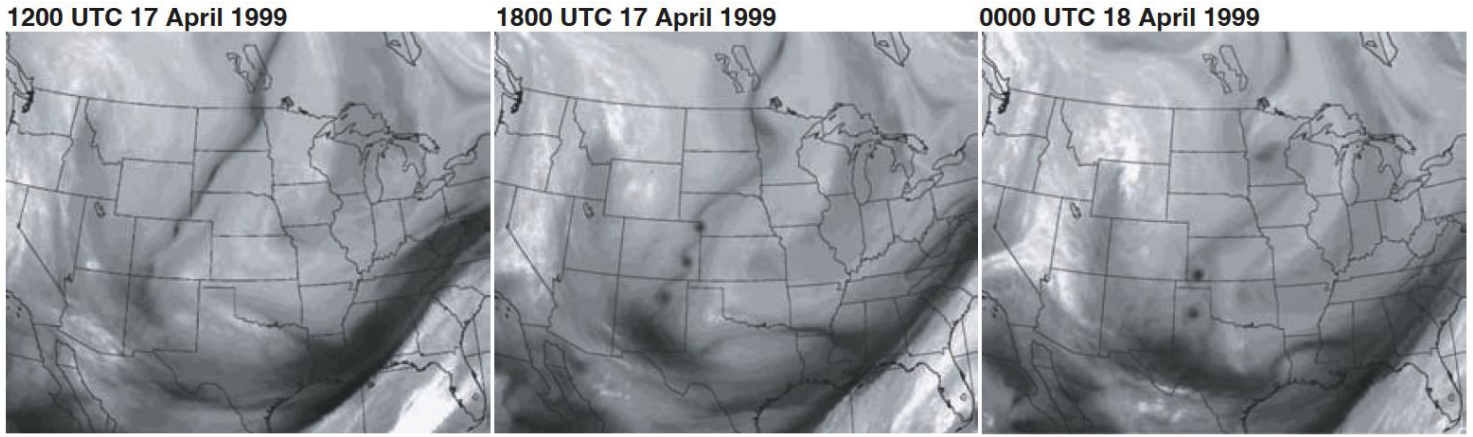

Figure 3.13 Water vapor satellite imagery from 1200–0000 UTC 17–18 April 1999 revealing the development of a series of vortices, most likely as a result of horizontal shear instability. (Adapted from Weinand [2000].)

Figure 3.14 This photograph of multiple waterspouts with a remarkably regular spacing strongly suggests that horizontal shear instability may have played a role in their formation. The image was obtained off the coast of Italy during the early spring of 2001. Photograph by Roberto Giudici.

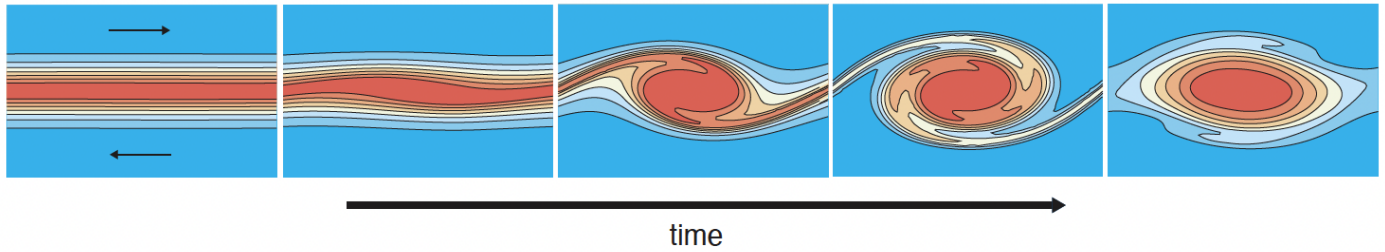

Figure 3.15 Idealized numerical simulation illustrating the effects of inflection-point instability. Time advances from left to right. Shading denotes vorticity magnitude. Warm (cool) colors indicate large (small) vorticity values. The mean wind direction is indicated by the arrows in the first panel. If instability is present and the high-vorticity interface is perturbed, the perturbation amplifies until the interface folds over on itself, leading to wave breaking and a transformation of what was initially a linear corridor of large vorticity into discrete patches of large vorticity. (Adapted from numerical simulation output provided by Brian Fiedler.)

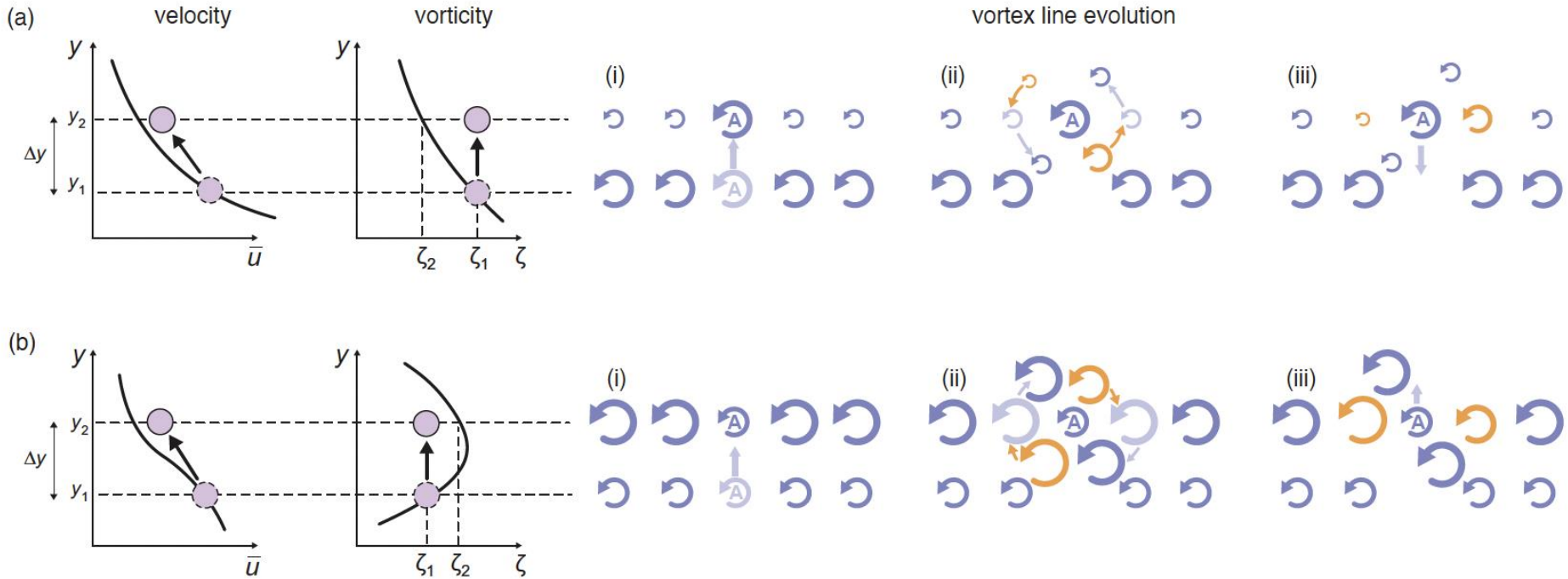

Figure 3.18 Schematic of a displaced vortex line A in a two-dimensional parallel flow (a) without and (b) with an inflection point in the velocity profile. The evolution of vortex lines is shown on the right. The sense of rotation induced by a vortex line is shown with arrows, with the size of the arrows increasing with increasing vorticity magnitude. Frame (i) shows the vortex line distribution immediately after vortex line A has been displaced. The light purple arrows indicate the prior position of vortex line A and the direction of its displacement. Frame (ii) shows the motion of the vortex lines initially at $y = y_2$ induced by vortex line A. The light purple arrows indicate the prior position of the vortex lines and the direction of their motion. The rotation associated with two additional vortex lines influenced by vortex line A, originally at $y = y_1 + \Delta y/2$ and $y = y_2 + \Delta y/2$, is indicated with orange arrows (these vortex lines are not shown in (i) in order to limit clutter). Frame (iii) shows the distribution of vortex lines a little later and the direction toward which vortex line A is accelerated. (Adapted from Brown [1972b] and based on the explanation provided by Lin [1945].)

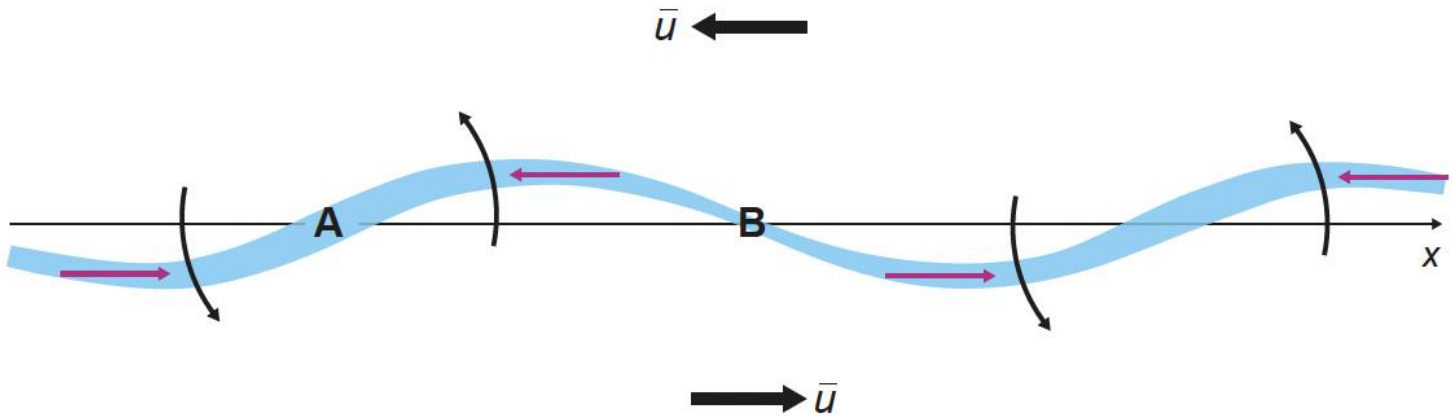

Figure 3.19 Growth of a sinusoidal perturbation on an initially uniform vortex sheet. The local sheet strength is indicated by the thickness of the sheet. The base state wind is indicated with the bold black arrows. The magenta arrows above and below the x axis indicate the direction of the induced vorticity movement along the sheet, concentrating vorticity at points such as A and depleting the vorticity at points such as B. The thick black arrows indicate the sense of rotation associated with the vortices that develop at points such as A. (Adapted from Batchelor [1967].)

Horizontal shear instability

Barotropic vorticity equation

$$\frac{\partial \zeta}{\partial t} + u\frac{\partial \zeta}{\partial x} + v\frac{\partial \zeta}{\partial y} + v\beta = 0, \qquad (3.68)$$

Linearized version

$$\left(\frac{\partial}{\partial t} + \overline{u}\frac{\partial}{\partial x}\right)\nabla_{\mathrm{h}}^2\Phi' + \frac{\partial \Phi'}{\partial x}\left(\beta - \frac{\partial^2 \overline{u}}{\partial y^2}\right) = 0. \qquad (3.69)$$

Consider a wavelike solution $\Phi' = \hat{\Phi}(y)\mathrm{e}^{ik(x-ct)}$,

Rayleigh equation

$$\frac{\partial^2 \Phi'}{\partial y^2} - k^2\Phi' + \frac{\left(\beta - \frac{\partial^2 \overline{u}}{\partial y^2}\right)}{\overline{u} - c}\Phi' = 0.$$

Necessary condition

$$c_{\mathrm{i}}\int_{-L}^{L} |\Phi'|^2 \frac{\left(\beta - \frac{\partial^2 \overline{u}}{\partial y^2}\right)}{|\overline{u} - c|^2}\mathrm{d}y = 0. \qquad (3.76)$$

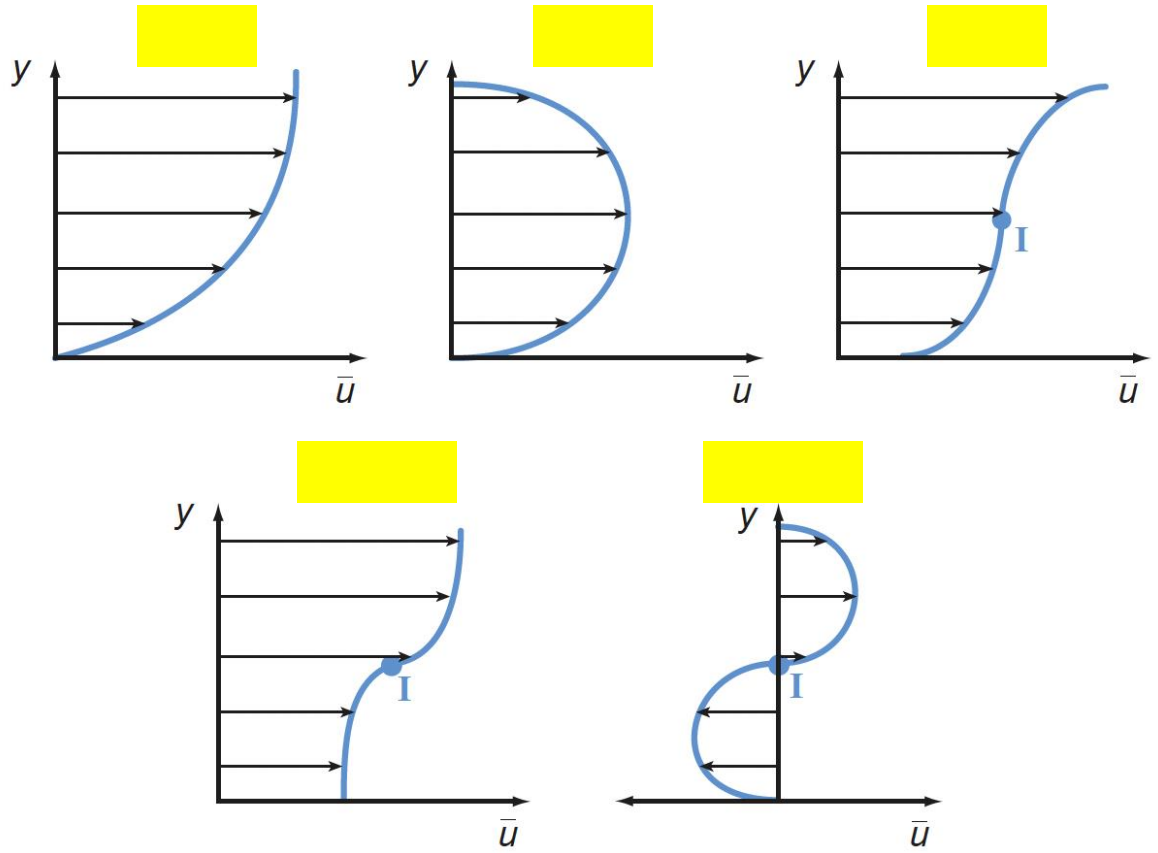

Figure 3.20 Horizontal wind profiles stable and unstable to small perturbations. Inflection points in the wind profiles are denoted with the letter 'I.' (Adapted from Kundu and Cohen [2008].)

Necessary condition

$$c_i \int_{-L}^{L} |\Phi'|^2 \frac{\left(\beta - \frac{\partial^2 \bar{u}}{\partial y^2}\right)}{|\bar{u} - c|^2} dy = 0.$$